Biochimica et Biophysica Acta 1840 (2014) 701–706

Contents lists available at ScienceDirect

Biochimica et Biophysica Acta

journal homepage: www.elsevier.com/locate/bbagen

Interaction of metal nanoparticles with recombinant arginine kinase from *Trypanosoma brucei*: Thermodynamic and spectrofluorimetric evaluation

O.S. Adeyemi, C.G. Whiteley *

Department of Biochemistry, Microbiology & Biotechnology, Rhodes University, Grahamstown, South Africa

ARTICLE INFO

Article history:
Received 24 July 2013
Received in revised form 21 September 2013
Accepted 25 October 2013
Available online 1 November 2013

Keywords:
Metal nanoparticle
Thermodynamic fluorimetric analysis
Trypanosomiasis
Arginine kinase

ABSTRACT

Background: Trypanosoma brucei, responsible for African sleeping sickness, is a lethal parasite against which there is need for new drug protocols. It is therefore relevant to attack possible biomedical targets with specific preparations and since arginine kinase does not occur in humans but is present in the parasite it becomes a suitable target.
Methods: Fluorescence quenching, thermodynamic analysis and FRET have shown that arginine kinase from *T. brucei* interacted with silver or gold nanoparticles.
Results: The enzyme only had one binding site. At 25 °C the dissociation (K_d) and Stern–Volmer constants (K_{SV}) were 15.2 nM, 0.058 nM^{-1} [Ag]; and 43.5 nM, 0.052 nM^{-1} [Au] and these decreased to 11.2 nM, 0.041 nM^{-1} [Ag]; and 24.2 nM, 0.039 nM^{-1} [Au] at 30 °C illustrating static quenching and the formation of a non-fluorescent fluorophore–nanoparticle complex. Silver nanoparticles bound to arginine kinase with greater affinity, enhanced fluorescence quenching and easier access to tryptophan molecules than gold. Negative ΔH and ΔG values implied that the interaction of both Ag and Au nanoparticles with arginine kinase was spontaneous with electrostatic forces. FRET confirmed that the nanoparticles were bound 2.11 nm [Ag] and 2.26 nm [Au] from a single surface tryptophan residue.
Conclusions: The nanoparticles bind close to the arginine substrate through a cysteine residue that controls the electrophilic and nucleophilic characters of the substrate arginine–guanidinium group crucial for enzymatic phosphoryl transfer between ADP and ATP.
General significance: The nanoparticles of silver and gold interact with arginine kinase from *T. brucei* and may prove to have far reaching consequences in clinical trials.

1. Introduction

Among the biomedical target molecules which have been identified as possible drug targets in African sleeping sickness (trypanosomiasis) is arginine kinase (AK), a phosphotransferase enzyme responsible for the reversible formation of phosphoarginine using L-arginine and ATP as substrates [Fig. 1] [1]. Phosphoarginine can act as an emergency reservoir, not only of ATP but also for inorganic phosphate [2–5].

The African disease is caused by the parasite *Trypanosoma brucei* while an equivalent malady in Latin America – Chagas disease – is caused by *Trypanosoma cruzi* [6–8] and both are fatal unless treated. Unfortunately current treatments have limited efficacy, unwanted toxicity, an emergence of resistant strains of trypanosomes, unsuccessful efforts at vaccine development and the absence of effective anti-trypanosomal therapies coupled with antigenic variation. Consequently there is an ongoing urgent requirement for innovative strategies and the development of new drugs to combat the diseases.

The enzyme AK is absent in humans [9], a fact that makes it the attractive target choice for trypanocide development. Furthermore there is an increased activity of AK in trypanosomes when linked to oxidative stress and since the trypanosomes are being constantly exposed to the pro-oxidants in the blood of mammalian host during their life-cycle the decrease in AK activity would present serious consequences to the growth and survival of the parasites. In light of this, compounds that selectively inhibit AK are desirable and should become candidates for early development of trypanocides.

The nanoscale size of metal nanoparticles allows their unique and remarkable properties to be exploited within the nanomedical fraternity and from our own laboratories have resolved several medical challenges in both infectious (malaria) [10,11] and neurodegenerative

* Corresponding author at: Department of Biochemistry, Microbiology and Biotechnology, Rhodes University, P.O. Box 94, Grahamstown 6140, South Africa. Tel.: +27 46 6038085; fax: +27 46 6223984.
E-mail address: C.Whiteley@ru.ac.za (C.G. Whiteley).

0304-4165/$ – see front matter © 2013 Elsevier B.V. All rights reserved.
http://dx.doi.org/10.1016/j.bbagen.2013.10.038

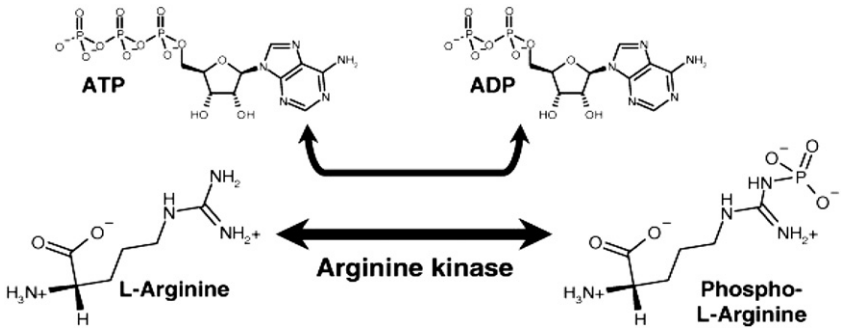

Fig. 1. Enzymatic reaction for arginine kinase.

diseases (Alzheimer) [12–14]. The present study investigates, from thermodynamic and spectrofluorimetric points of view, the interaction of silver and/or gold nanoparticles with a recombinant form of AK enzyme obtained from *T. brucei* (TbAK).

2. Materials and methods

2.1. Materials

Genomic DNA of *T. brucei* (T927) was a gift from Professor Ullman, Department of Biochemistry & Biophysics, Oregon Health & Science University, Portland, Oregon, USA. Enzymes and PCR reagents were provided by Thermo Fischer Scientific, USA. A Bioflux kit was obtained from Separation Scientific (South Africa). Oligonucleotides and primers were from the Integrated DNA Technology (IDT), USA. The clone JET PCR kit, pSMART and pET-28b (+) as well as the BL21 DE3 and JM 109 strains of *Escherichia coli* were obtained from Fermentas Life Sciences (USA). Absorbance spectroscopy was performed with a Synergy Mx Monochromator Multi-Mode Microplate Reader (Biotek Instruments, Inc., USA). All reagents were of analytical grade and obtained from domestic suppliers unless otherwise stated.

2.2. Assay for TbAK [15]

Enzyme extract (20 μl) was incubated (5 min, 30 °C) with L-arginine (10 mM), ATP (5 mM), mercaptoethanol (10 mM), and $MgSO_4$ (200 mM) in Tris–HCl buffer (100 mM, pH 8.6) in a final volume of 170 μl. Trichloroacetic acid (180 μl, 2.5%) was then added and the whole mixture was heated (100 °C, 2 min) to stop the reaction. After cooling the mixture was treated with ascorbic acid/ammonium molybdate (9%, 100 μl), left for colour development (5 min), and the absorbance was read at 700 nm. The amount of phosphate released was measured by means of a standard curve as one unit of TbAK activity is the amount of enzyme that catalyses the formation of 1 μmol inorganic phosphate per minute per ml.

2.3. Cloning, expression, purification of TbAK [15]

Primers of TbAK used to amplify the open reading frame of the TbAK gene were CAT ATG GGC TTC GGA TCA TCA AAA CCC; (forward; NdeI restriction site underlined) and CTC GAG CTG TTC CAC GTA CCT GC; (reverse; XhoI restriction site underlined). The PCR reaction was carried out with amplification conditions as follows: Initial denaturation (98 °C,3 min), 40 cycles of denaturation (98 °C, 30 sec), annealing (62 °C, 30 sec; 72 °C, 10 sec), and elongation (72 °C, 60 sec) in a Biorad T100 thermal cycler. The 1000 bp product was excised, gel purified using a Bioflux kit then phosphorylated and blunt ligated into a pSMART vector using a T4 DNA ligase and finally transformed into JM 109 cells. The plasmid that contained the TbAK was gel purified using the Bioflux kit, sequenced and showed 100% identity with the *T. brucei* expressed product (Accession number — XP_826998.1) and a high identity with other related guanidino kinases. The plasmid was double digested and a fragment between NdeI and XhoI restriction sites containing the TbAK gene was excised from the plasmid and subcloned into a pET-28b (+) expression vector previously treated with NdeI and XhoI. This plasmid transcribes under the control of the T7 promoter and includes a polyhistidine tag. This was transformed into BL21 DE3 cells, grown overnight, at 37 °C, in 50 ml LB culture medium containing kanamycin after which an aliquot (5.0 ml) was transferred into a 2 l flask containing auto-media culture (500 ml). This was grown (20 °C, 150 rpm, 36 h) and the cells harvested (6000 ×*g*, 10 min), washed twice with Tris buffered saline (Tris-HCl, 50 mM; NaCl, 150 mM; pH 7.5) and lysed (freeze-thawed [−80 °C/4 °C; 2 cycles]) in lysis buffer [NaH_2PO_4 buffer (50 mM, pH 7.6) containing NaCl (300 mM), glycerol (10%), Tween (0.25%), imidazole (10 mM), mercaptoethanol (10 mM), phenylmethylsulphonylfluoride (1 mM)]. The lysed cells were centrifuged (2700 ×*g*, 30 min) and the supernatant was centrifuged (100,000 ×*g*, 90 min) after which the supernatant (150 ml) was loaded onto a Ni–nitrilotriacetic acid affinity column previously washed with the same lysis buffer. The fusion protein was eluted with increasing amounts of imidazole (0–500 mM) in Hepes buffer (10 mM, pH 7.5) and concentrated using vivaspin (GE Healthcare, Sweden) and then purified by FPLC on a Superdex 200 HR 10/30 column with Hepes buffer (25 mM, pH 7.6) containing glycerol (15%), EDTA (0.1 M), KCl (1 M) at a flow rate of 1 $ml \cdot min^{-1}$. Proteins were resolved by SDS-PAGE in order to confirm purity of fractions before pooling. All purification procedures were carried out at 4 °C.

2.4. Characterisation of TbAK

The purity of TbAK was assessed by SDS-PAGE analysis and its optimum temperature, thermal stability, pH optimum and kinetic parameters (K_m and V_{max}) were established [15].

2.5. Synthesis and characterization of gold and silver nanoparticles

Gold and silver nanoparticles were synthesised, respectively, from either $AuCl_3$ or $AgNO_3$ and stabilized with tannic acid/polyvinylpyrrolidone. The pale yellow solution (Ag-NPs) and the wine red solution (Au-NPs) were filtered using the 0.22 μM filter and characterised by UV/Vis spectrophotometry, inductively coupled plasma optical emission spectrometry (ICP-OES), energy dispersive X-ray spectroscopy (EDX) and transmission electron microscopy (TEM) [15].

2.6. Fluorimetric analysis of the interaction of nanoparticles with TbAK

Structural changes induced in TbAK by the interaction of the silver/gold nanoparticles were determined spectrofluorimetrically at an excitation wavelength of 295 nm, the wavelength at which tryptophan absorbs, and an emission wavelength of 350 nm. The change in fluorescence of a solution was monitored at 25 °C, over 10 min, as increasing

concentrations of the respective nanoparticles (0–50 nM) were added to a reaction mixture of TbAK (5 μl) in triethanolamine buffer (pH 7.4, 10 mM) containing NaCl (100 mM) in a final volume of 200 μl. All fluorescence quenching experiments were performed at 25 °C [298 K] and 30 °C [303 K].

2.7. Statistical analyses

All analyses were carried out in triplicate and values were reported as the means with standard deviation $p < 0.05$ versus controls. Analysis of variance was conducted using Statistica for Windows, version 8 (Statsoft Inc.) and Microsoft Excel 2010.

3. Results and discussion

3.1. Binding site for nanoparticles on TbAK

The binding parameters of nanoparticles for TbAK can be analysed accordingly [Eq. (1)].

$$\mathbf{Log}[(\mathbf{Fo}-\mathbf{F})/\mathbf{F}] = \mathbf{logKa} + \mathbf{nlog}[\mathbf{Q}] \quad (1)$$

where Fo and F are the fluorescent intensities of TbAK in the absence and presence of either silver or gold nanoparticles respectively; Q is the concentration of nanoparticles; 'n' is the number of binding sites (on the purified enzyme available for the particles), and Ka is the association constant [and its reciprocal dissociation constant (Kd)]. Both 'n' and Ka were estimated, respectively, from the slope of the linear regressions and the intercept on the log [(Fo − F) / F] axis [Fig. 2] [16]. For both Ag and Au nanoparticles only 1 binding site was available. The values obtained for the binding constants (K_d) [15.2 nM for Ag; 43.5nM for Au nanoparticles] indicated a strong affinity between TbAK and the nanoparticles. As the temperature increased from 25 °C [298 K] to 30 °C [303 K] these K_d values changed slightly to 11.12 nM (Ag); 24.21 nM (Au).

3.2. Fluorescence quenching analysis

The binding of the nanoparticles caused a quenching in the tryptophan fluorescence of TbAK [Fig. 3a; b] with linearity in the Stern–Volmer plots implying that one, or more, tryptophan residues are close to the binding site. The possible quenching mechanism can be interpreted from the fluorescence analysis data and analysed according to the

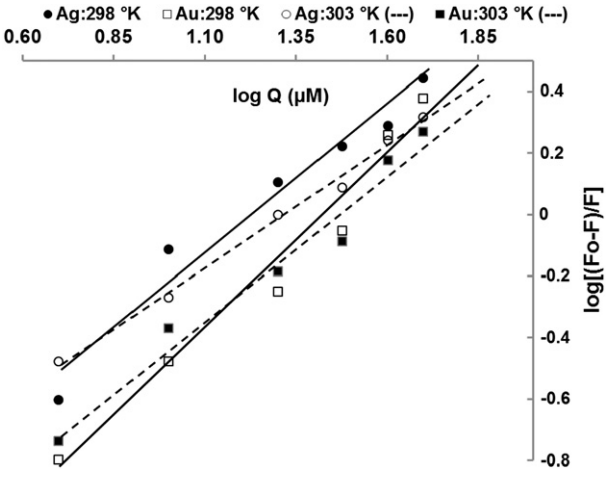

Fig. 2. Hill plots of log [(Fo − F)/F] versus log [Q] for the binding of Ag and Au nanoparticles (0–50 nM) with TbAK (5 μl) in triethanolamine buffer (pH 7.4, 10 mM) containing NaCl (100 mM) in a final volume (200 μl) at two different temperatures (●), [Ag − 298 K], (● --), [Ag − 303 K]; (■), [Au − 298 K], (■ --), [Au − 303 K]. $\lambda_{ex} = 295$ nm and $\lambda_{em} = 350$ nm.

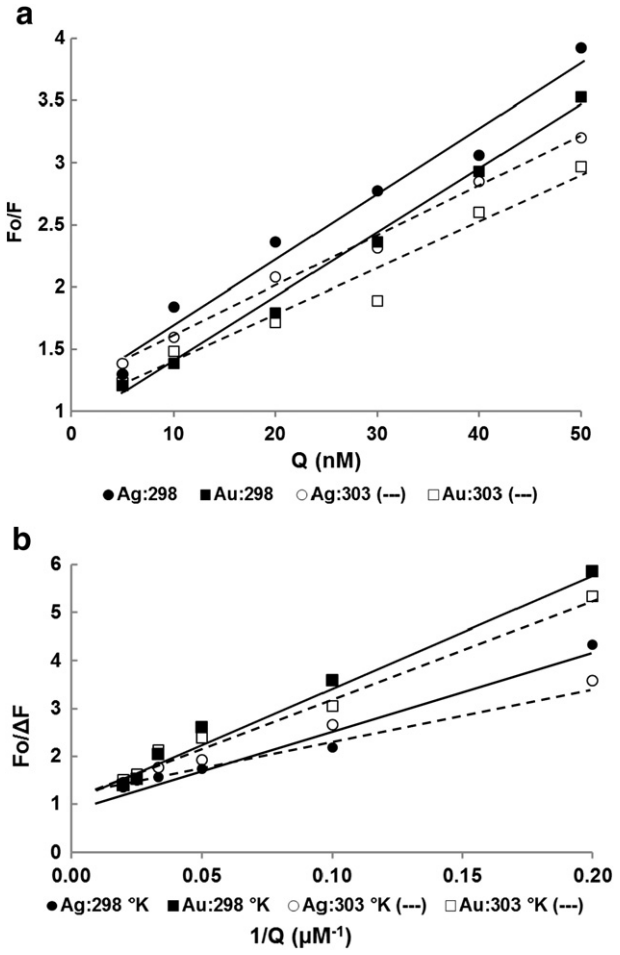

Fig. 3. a: Stern–Volmer plots for fluorescence quenching for the binding of Ag and Au nanoparticles (0–50 nM) with TbAK (5 μl) in triethanolamine buffer (pH 7.4, 10 mM) containing NaCl (100 mM) in a final volume (200 μl) at two different temperatures (●), [Ag − 298 K], (● --), [Ag − 303 K]; (■), [Au − 298 K], (■ --), [Au − 303 K]. $\lambda_{ex} = 295$ nm and $\lambda_{em} = 350$ nm. **b**: Double reciprocal plots (modified Stern–Volmer) for the binding of Ag and Au nanoparticles (0–50 nM) with TbAK (5 μl) in triethanolamine buffer (pH 7.4, 10 mM) containing NaCl (100 mM) in a final volume (200 μl) at two different temperatures (●), [Ag − 298 K], (● --), [Ag − 303 K]; (■), [Au − 298 K], (■ --), [Au − 303 K]. $\lambda_{ex} = 295$ nm and $\lambda_{em} = 350$ nm.

Stern–Volmer equations [Eqs. (2), (3)]. The Stern–Volmer constant (K_{SV}) was estimated from the slope of the linear regression and θ, the fraction of tryptophan residues near the surface of the enzyme, from the reciprocal of the y-intercept [Fig. 3b].

$$\mathbf{Fo}/\Delta\mathbf{F} = \mathbf{1}/(\theta\mathbf{KsvQ}) + \mathbf{1}/\theta \quad (2)$$

$$\mathbf{Fo}/\mathbf{F} = \mathbf{1} + \mathbf{KsvQ} \quad (3)$$

where ΔF = Fo − F. The 'y intercept' from the Stern–Volmer plots [Fig. 3a] was equivalent to 1, thereby indicating that fluorescence was only due to internal quenching by the nanoparticle and not the interplay of other fluors in solution which may result in external quenching. Respective K_{SV} values for Ag- and Au-nanoparticles were 0.058 nM^{-1} and 0.052 nM^{-1}. As the temperature changed from 25 °C [298 K] to 30 °C [303 K] the respective K_{SV} values decreased to 0.041 nM^{-1} and 0.039 nM^{-1} [Fig. 3a] illustrating that the quenching by the nanoparticles must be classified as static supported by the formation of a non-fluorescent fluorophore–nanoparticle complex [17,18].

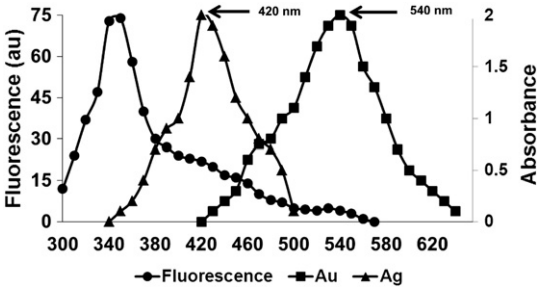

Fig. 4. Spectral overlap of fluorescence emission spectrum of TbAK and absorbance spectra for Au and Ag nanoparticles with plasmon resonance maxima indicated at 420 nm and 540 nm.

3.3. Fluorescence energy transfer (FRET)

Fluorescence quenching of Trp within the TbAK active site can also be used by a process of energy transfer (FRET) that allows for the measurement of the relative distance (r) between this tryptophan and the bound nanoparticle according to Försters theory [19]. Since there is spectral overlap of the fluorescence emission spectrum of TbAK and the UV absorption spectra of the Ag and Au nanoparticles [Fig. 4] this distance (r) can be calculated from the efficiency of energy transfer (E) [Eq. (4)].

$$\mathbf{E = 1 - F/Fo = Ro^6/\left(Ro^6 + r^6\right)} \quad (4)$$

$$\mathbf{Ro^6 = 8.79 \times 10^{-25}\kappa^2\eta^{-4}\varphi\left[\sum\int F_\lambda \cdot \varepsilon_\lambda \cdot \lambda^4 \cdot \Delta\lambda\right]/\left[\sum\int F_\lambda \cdot \Delta\lambda\right]} \quad (5)$$

where Ro = Förster distance when efficiency of transfer is 50% and depends on the relative orientation of the tryptophan and nanoparticle (κ), the refractive index of the medium (η), the quantum fluorescence yield (φ), F_λ is the fluorescence intensity of the tryptophan at wavelength (λ) and ε_λ is the molar absorption coefficient of the nanoparticle at wavelength (λ); the integral overlap of the fluorescence emission spectrum of TbAK and the absorption spectrum of the Ag nanoparticle is represented within the integration symbols [Eq. (5)].

Assuming $\kappa^2 = 0.667$; $\varphi = 0.118$; and $\eta = 1.336$ [12,20] then from Eqs. (4) and (5), Ro and r for Ag and Au nanoparticles are estimated as 2.18, 2.11 nm and 2.35, 2.26 nm respectively. According to literature, any value for this distance (r) that is less than 10 nm and falls between 0.5 and 1.5 of the Ro value indicates a high probability that fluorescence transfer is taking place [21].

An in-depth molecular modelling and docking study of the interaction and binding of these nanoparticles to TbAK is currently on going and will be reported elsewhere. As far as we were aware no crystallographic structure for arginine kinase from *T. brucei* had been deposited in the Protein Data Bank. On the other hand that for *T. cruzi* [TcAK] had been reported [22] with 82% analogy [23] to *T. brucei*. The analysis of the primary structure of TcAK [PDB ID: 2J1Q] reveals only 2 tryptophan residues — one buried near the ATP/ADP active binding site [Trp^{221}] and one on the surface of the enzyme [Trp^{104}] [24]. FRET studies confirmed that the nanoparticles quenched the fluorescence of only one tryptophan residue, most probably the surface Trp^{104}, as θ [Eq. (2)] [Fig. 3b] was equal to 1 for both types of nanoparticles and at both temperatures.

The interatomic distance between NH_1 of the arginine substrate and the aromatic ring of Trp^{104} is 22.2 Å (2.22 nm) [Fig. 5] while that for Trp^{221} is 15.1 Å (1.51 nm). Furthermore a thiolate sulphur atom from Cys^{271} is only 3.3 Å from this reactive N_1. The present findings from FRET analysis indicate that the distances between Trp^{104} and the bound nanoparticles are 2.11 nm and 2.26 nm for Ag and Au respectively.

It is well known from our other studies on apoferritin/ferroxidase, GroEL/ATPase and comparative study with human/*Plasmodium falciparum* superoxide dismutase (hSOD/PfSOD) [10,11,25] that both Ag and Au nanoparticles have not only catalytic properties but a strong affinity to the thiol (SH) group of cysteine residues. From a structural and mechanistic point of view the distance between critical amino acid residues within the active regions of these enzymes was about 2.5–4.0 Å well within the range for the nanoparticles to bind. This affected the nucleophilic character of these amino acids altering

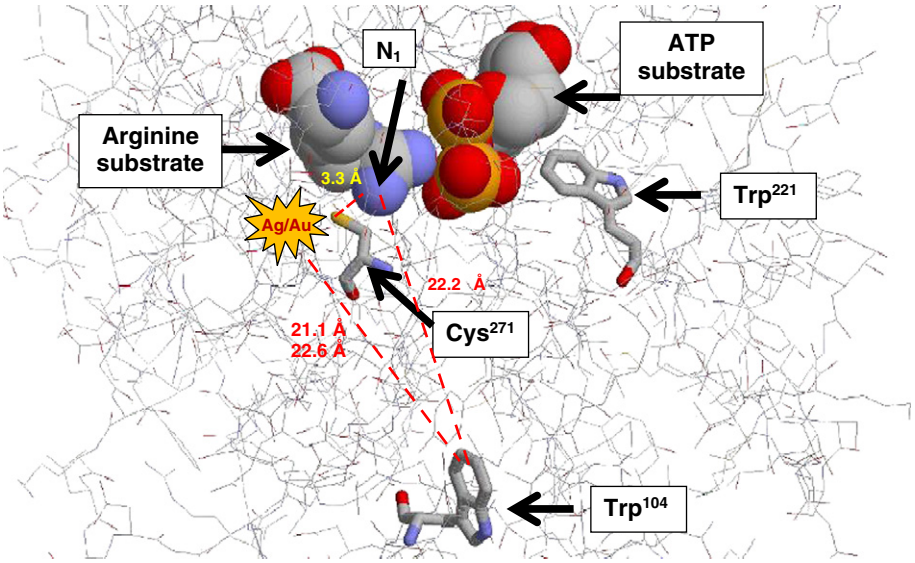

Fig. 5. Proposed structure of the binding sites for TbAK showing the interaction of silver/gold nanoparticles through Cys^{271}, interfering with N_1 of the arginine substrate. The interatomic distance between the thiolate atom of Cys^{271} and N_1 of the arginine substrate is 3.3 Å. The interatomic distance between Trp^{104} and N_1 is 22.2 Å while that distance between Trp^{104} and bound Ag/Au nanoparticles is 21.1 Å and 22.6 Å respectively. Nitrate not shown.

the binding of Fe^{2+} (ferroxidase) and/or Cu^{+} (hSOD) to the nanoparticles and consequently changing the rate of electron removal and oxidation to Fe^{3+} and/or Cu^{2+}. The interaction of the nanoparticles facilitates the formation of a respective hydrolysis product (FeOOH; H_2O_2). In hSOD Cys^{57} and Cys^{146} are 2.08 Å apart and nanoparticle binding changes the conformation of the reactive core and changes the rate of addition of oxidant. These two amino acids are not present in *Pf*SOD. With respect to ferritin/ferroxidase — three Cys^{126} residues from three different chain are juxtaposed within 3.6 Å from the Fe^{2+}/Fe^{3+} core suggesting that the gold/silver nanoparticles interact at these positions and with exposed-SH groups leading to altered activity.

Consequently, based upon this discussion, it is well within the realm of possibility that the nanoparticles would interact with the sulphur atom of Cys^{271} [Fig. 5]. This would decrease its electronegativity and, in turn, decrease the nucleophility of the N_1 of the arginine substrate towards attack on the ϒ-phosphoryl group of ATP. With the enzymatic formation of ATP, a blocking of the thiolate by nanoparticles would prevent its acceptance of a proton from the arginine guanidinium group decreasing the overall phosphoryl transfer to ADP.

3.4. Thermodynamic analysis

In order to elucidate the interactive forces between TbAK and Au/Ag nanoparticles temperature-dependent thermodynamic parameters were calculated according to van't Hoff [Eq. (6)]; ΔG was also estimated [Eq. (7)].

$$\mathbf{ln K_{sv}} = -(\Delta \mathbf{H}/\mathbf{RT}) + (\Delta \mathbf{S}/\mathbf{R}) \quad (6)$$

$$\Delta \mathbf{G} = \Delta \mathbf{H} - \mathbf{T}\Delta \mathbf{S} \quad (7)$$

where R = gas constant (8.314 J mol^{-1} K^{-1}); ΔH = enthalpy change, ΔS = entropy change, ΔG = free energy change and K_{sv} = Stern–Volmer binding constant at the corresponding temperature (T, K). Since the Stern–Volmer plot was linear [Fig. 3a] and the quenching mechanism by the nanoparticles classified as a static one K_{SV} can be equated to K_a [18].

According to enthalpy change (ΔH) and entropy change (ΔS), the model of interaction between any ligand and protein can be concluded as: (1) ΔH > 0 and ΔS > 0 are indicative of hydrophobic forces; (2) ΔH < 0 and ΔS < 0 are indicative of Van de Waals interactions and hydrogen bonds; and (3) ΔH < 0 and ΔS > 0 are indicative of electrostatic interactions [26,27]. Consequently negative ΔH, positive ΔS and negative ΔG values from the interaction of both Ag and Au nanoparticles with TbAK (Table 1) implied that not only were electrostatic forces operative during the binding but also the interaction was spontaneous and governed by large thermodynamically favourable entropies, confirmed by the large positive values of ΔS: 152.74 J mol^{-1} K^{-1}, (Ag nanoparticles) and 116.59 J mol^{-1} K^{-1}, (Au nanoparticles).

4. Conclusions

A thorough investigation of the interaction of silver and gold nanoparticles with TbAK in terms of thermodynamic and spectrofluorimetric analyses has been undertaken. Binding constants obtained were consistent with a spontaneous static quenching, governed by large thermodynamically favourable positive entropies, and negative ΔH and ΔG values that supported electrostatic forces in operation. FRET analysis estimated the binding distance between Trp^{104} and Ag nanoparticle to be 2.11 nm while that for Au to be 2.26 nm.

Table 1
Thermodynamic parameters estimated for the interaction between arginine kinase of *Trypanosoma brucei* (TbAK) and Ag/Au nanoparticles at two different temperatures.

Nanoparticle	T (K)	ΔH (kJ·mol^{-1})	ΔG (kJ·mol^{-1})	ΔS (J mol^{-1} K^{-1})
Ag	298	−52.55	−98.07	152.74
	303		−98.83	
Au	298	−42.08	−76.82	116.59
	303		−77.38	

Acknowledgements

This research was supported by the National Research Foundation (NRF) South Africa. We want to thank Prof. Buddy Ullman (Department of Biochemistry & Biophysics, Oregon State University, USA) and Dr. Jacqui van Marjwik (Postdoctoral fellow, Department of Biochemistry, Microbiology & Biotechnology, Rhodes University, Grahamstown, South Africa).

References

[1] C.A. Pereira, G.D. Alonso, M.C. Paveto, M.M. Flawiá, H.N. Torres, L-arginine uptake and L-phosphoarginine synthesis in *Trypanosoma cruzi*, J. Eukaryot. Microbiol. 46 (6) (1999) 566–570.
[2] C.A. Pereira, G.D. Alonso, S. Ivaldi, A. Silver, M.J. Alves, H.N. Torres, M.M. Flawiá, Arginine kinase overexpression improves *Trypanosoma cruzi* survival capability, FEBS Lett. 554 (1–2) (2003) 201–205.
[3] L.D. Andrews, J. Graham, M.J. Snider, D. Fraga, Characterisation of a novel bacterial arginine kinase from *Desulfotalea psychrophila*, Comp. Biochem. Physiol. B Biochem. Mol. Biol. 150 (3) (2008) 312–319.
[4] W.R. Ellington, Evolution and physiological roles of phosphagen system, Annu. Rev. Physiol. 63 (2001) 289–325.
[5] K. Uda, N. Fujimoto, Y. Akiyama, K. Mizuta, K. Tanaka, W.R. Ellington, T. Suzuki, Evolution argine kinase gene family, Comp. Biochem. Physiol. D Genomics Proteomics 1 (2) (2006) 209–218.
[6] F. Canonaco, U. Schlattner, P.S. Pruett, T. Wallimann, U. Sauer, Functional expression of arginine kinase improves recovery from pH stress of *Escherichia coli*, Biotechnol. Lett. 25 (13) (2003) 1013–1017.
[7] F. Canonaco, U. Schlattner, P.S. Pruett, T. Wallimann, U. Sauer, Functional expression of phosphagen kinase systems confers resistance to transient stresses in *Saccharomyces cerevisiae* by buffering the ATP pool, J. Biol. Chem. 277 (35) (2002) 31303–31309.
[8] C.A. Pereira, L.A. Bouvier, M.M. Cámara, M.R. Miranda, Singular features of Trypanosomatids' phosphotransferases involved in cell energy management, Enzyme Res. (2011), http://dx.doi.org/10.4061/2011/576483.
[9] M.R. Miranda, G.E. Canepa, L.A. Bouvier, C.A. Pereira CA, *Trypanosoma cruzi*: oxidative stress induces arginine kinase expression, Exp. Parasitol. 114 (4) (2006) 341–344.
[10] A. Sennuga, J. van Marwijk, C.G. Whiteley, Ferroxidase activity of apoferritin is increased in the presence of platinum nanoparticles, Nanotechnology (2012), http://dx.doi.org/10,1088/0957-4484/23/3/035102.
[11] A. Sennuga, J. van Marwijk, C.G. Whiteley, Multiple fold increase in activity of ferroxidase–apoferritin complex by silver and gold nanoparticles, Nanomed. Nanotechnol. Biol. Med. 9 (2) (2013) 185–193.
[12] E.R. Padayachee, C.G. Whiteley, Spectrofluorimetric analysis of amyloid peptides with neuronal nitric oxide synthase: implications in Alzheimer's disease, Biochim. Biophys. Acta 1810 (2011) 1136–1140.
[13] E.R. Padayachee, C.G. Whiteley, Interaction of glycine zipper fragments of Aβ-peptides with neuronal nitric oxide synthase: kinetic, thermodynamic and spectrofluorimetric analysis, Neuropeptides 47 (2013) 171–178.
[14] E.R. Padayachee, N. Ngqwala, C.G. Whiteley, Association of β-amyloid peptide fragments with neuronal nitric oxide synthase: implications in the etiology of Alzheimers disease, Enzyme Inhib. Med. Chem. 27 (3) (2012) 356–364.
[15] O.S. Adeyemi, C.G. Whiteley, Interaction of nanoparticles with arginine kinase from *Trypanosoma brucei*: kinetic and mechanistic evaluation, Int. J. Biol. Macromol. 62 (2013) 450–456.
[16] M.X. Xie, X.Y. Xu, Y.D. Wang, Interaction between hesperetin and human serum albumin revealed by spectroscopic methods, Biochim. Biophys. Acta Gen. Subj. 1724 (1–2) (2005) 215–224.
[17] A.S. Al-Kady, M. Geber, M.M. Hussein, E.M. Ebeida, Structural and fluorescence quenching characterisation of hematite nanoparticles, Spectrochim. Acta 83 (2011) 398–405.
[18] D.E. Schlamadinger, D.J. Kats, J.E. Kim, Quenching of tryptophan fluorescence in unfolded cytochrome c: biophysics experiment for physical chemistry students, J. Chem. Educ. 87 (9) (2010) 961–964.
[19] T. Förster, Intermolecular energy migration and fluorescence, Ann. Phys. 2 (1948) 55–75.
[20] H. Wang, W. Zhu, X. Wang, Mechanism of inhibition of arginine kinase by flavonoids consistent with thermodynamics of docking simulation, Int. J. Biol. Macromol. 49 (5) (2011) 985–991.
[21] Y. Chen, J.D. Mills, A. Periasamy, Protein localization in living cells and tissues using FRET and FLIM, Differentiation 71 (2003) 528–554.

[22] P. Fernandez, A. Haouz, C.A. Pereira, C. Aguilar, P.M. Alzari, The crystal structure of *Trypanosoma cruzi* arginine kinase, Proteins 69 (2007) 209–214.
[23] C.A. Pereira, G.D. Alonso, H.N. Torres, M.M. Flawiá, Arginine kinase: a common feature for management of energy reserves in African and American flagellated trypanosomatids, J. Eukaryot. Microbiol. 49 (1) (2002) 82–85.
[24] X. Wu, W. Zhu, Z. Lü, Y. Xia, J. Yang, F. Zou, X. Wang, The effect of rutin on arginine kinase: inhibition kinetics and thermodynamics merging with docking simulation, Int. J. Biol. Macromol. 44 (2) (2009) 149–155.
[25] A. Sennuga, J. van Marwijk, A. Boshoff, C.G. Whiteley, Enhanced activity of chaperonin GroEL in the presence of platinum nanoparticles, J. Nanopart. Res. 14 (5) (2012), http://dx.doi.org/10.1007/s11051-012-0824-6.
[26] P.D. Ross, S. Subramanian, Thermodynamics of protein association reactions: forces contributing to stability, Biochemistry 20 (1981) 3096–3102.
[27] S. Strazza, R. Hunter, E. Walker, D.W. Darnall, The thermodynamics of bovine and porcine insulin determined by concentration difference spectroscopy, Arch. Biochem. Biophys. 238 (1985) 30–42.